Journal of Molecular Liquids 368 (2022) 120739

Contents lists available at ScienceDirect

Journal of Molecular Liquids

journal homepage: www.elsevier.com/locate/molliq

Thermodynamic assessment and microscale Raman spectroscopy of binary CO_2/CH_4 hydrates produced during replacement applications in natural reservoirs

Rita Giovannetti [a,*], Alberto Maria Gambelli [b], Andrea Rossi [a,*], Beatrice Castellani [b], Marco Minicucci [c], Marco Zannotti [a], Andrea Nicolini [b], Federico Rossi [b]

[a] School of Science and Technology, Chemistry Division, ChIP Research Center, University of Camerino, 62032 Camerino, Italy
[b] Engineering Department, University of Perugia, Via G. Duranti 93, 06125 Perugia, Italy
[c] School of Science and Technology, Physics Division, University of Camerino, 62032 Camerino, Italy

ARTICLE INFO

Article history:
Received 12 August 2022
Revised 15 October 2022
Accepted 1 November 2022
Available online 13 November 2022

Keywords:
Natural gas hydrates
CO_2/CH_4 replacement process
CO_2 capture and storage
CO_2 and CH_4 gas hydrates
Raman OH-stretching vibrations
SEM

ABSTRACT

The present research deals with the micro – scale characterization of sI hydrates containing a binary mixture of methane and carbon dioxide. The application of replacement strategies in natural hydrate reservoirs, always leads to the formation of "mixed" hydrates, whose mechanical and chemical properties are different from those of pure CH_4 and CO_2 hydrates. As a function of the technique used for the process and due to the variability of the systems, a wide range of different compositions and morphologies can be obtained and the current literature must be expanded, in order to achieve a wide and accurate experimental database of CO_2/CH_4 hydrate properties. In this work, binary CO_2/CH_4 hydrates binary CO_2/CH_4 hydrates were produced in a small – scale reactor and then supercooled, in order to favour their extraction from the reactor and their stability at environmental conditions for a certain period of time. The gas hydrates, prepared with CO_2 hydrates of pure water and with CH_4 and CO_2 mixtures, also in the presence of specific sands, were ex situ analysed by the use Raman-spectroscopy that confirmed the gas uptake in the hydrate structures by identification of the fingerprint of CH_4 and CO_2 occupancy in the hydrates. The characteristic of water inside the gas hydrates and the interaction between the host molecules and the lattice of water molecules was clarified. The different gas hydrates, analysed by Field Emission Scanning Electron Microscopy instrument equipped with "Coolstage head" under high vacuum condition, differed in morphology and surface features.

The analysis of water Raman spectra of the different GHs permitted to describe the relation between symmetric and asymmetric OHs bands, but also provided information about the characteristics of water inside the different GHs, showing that the least ordered water structure was that of GHs containing sand, while the most ordered one was present on binary CO_2/CH_4 hydrates.

1. Introduction

Gas hydrates (GHs) are ice – like crystalline compounds, whose structure is composed by water molecules, commonly referred as hosts [1]. The different solid cages contain gaseous molecules, defined as guests. Several gaseous species are capable to form hydrates: among them, methane and carbon dioxide. In the mid-1960, the existence of enormous natural deposits, diffused worldwide, was proved and natural gas hydrates started being considered as a potential new energy source [2]. Since 164 – 180 Nm^3 of methane can be enclathrated in only one cubic meter of hydrate, this source immediately gained a growing interest also as high – density energy source [3]. Natural hydrate reservoirs mainly occur in deep ocean sediments (≈ 97%) and in terrestrial permafrost (≈ 3%) [4,5]. In addition to energy production, gas hydrates and their formation/dissociation mechanism can be advantageously exploited in several applications of interest, such as energy storage, carbon dioxide storage (CCS), gas transportation, separation of gaseous mixtures into single components, climate change mitigation, seawater desalination, wastewater purification and so on [6,7].

However, the exploitation as energy source remains the most attractive option. According to recent estimations, the quantity of

* Corresponding authors.
E-mail addresses: rita.giovannetti@unicam.it (R. Giovannetti), andrea.rossi@unicam.it (A. Rossi).

https://doi.org/10.1016/j.molliq.2022.120739
0167-7322/

methane contained into natural hydrate reservoirs ranges from 10^{15} to 10^{17} m^3 [8]; such quantity is theoretically enough to produce more than twice the energy which can still be obtained from all the conventional energy sources, currently known and available, put together [9].

The results achieved in field tests proved that the process of methane production from natural gas hydrate, must be widely improved before being economically feasible and completely sustainable for the environment [10,11].

The most explored and applied techniques for methane recovery from hydrates are depressurization [12], thermal stimulation [13,14], chemical inhibitor injection [15], or a combination of them [16].

The first strategy is based on lowering the local pressure of the reservoir, while keeping the temperature constant, in order to move the local conditions outside from the stability zone for methane hydrates [17,18]. The efficiency of the depressurization technique mainly depends on the diffusion of pressure, the permeability of the reservoir and its saturation degree [19]. With thermal stimulation, the opposite action is exercised to obtain the same effect: the local temperature is increased, while pressure is kept constant. Depressurization and thermal stimulation are the most widespread techniques and show the highest energy produced/energy spent ratio [20]; especially when applied simultaneously. Hassanpouryouzband and co – workers asserted that, by itself, thermal stimulation is not a viable solution and must be combined with depressurization to become really effective [21]. Finally, the injection of chemical inhibitors allows to make the local thermodynamic conditions unfeasible for hydrates stability, without varying them [22].

Since 1980, a further potential solution was discovered [1]: the CO_2/CH_4 replacement process. Such method does not exclusively work on the recovery of methane, it also allows to perform carbon dioxide sequestration in form of hydrates [23]. The exchange process is favored by the capability of carbon dioxide molecules to form hydrates at milder conditions than those required for methane hydrates. The reason can be found in the lower enthalpy of formation for CO_2 hydrates. It means that, at the same thermodynamic conditions, the hydrates containing carbon dioxide are more stable [24]. Two different possibilities, for CO_2/CH_4 replacement, exist: (i) the initial dissociation of methane hydrates, with the following formation of carbon dioxide hydrates [25,26], or (ii) the direct exchange between the two gaseous species, within the already formed water cages [27]. The second solution is preferred because it avoids the production of water and preserve the morphology of the sediment, thus reducing the risk of hydrogeological instability [28]. In addition, the exchange ratio between the two species is theoretically equal to one.

However, some limiting aspects must be considered and discussed. Even if these species are trapped within the same typology of crystalline ratio, the difference in size leads to a different filling of the cavities. The cubic structure I is composed by two different types of cages: the relatively small – size pentagonal dodecahedron (5^{12}) and the relatively large – size tetrakaidecahedron ($5^{12}6^2$) [1]. The cage occupancy ratio for methane molecules, θ_L/θ_S, is equal to 1.26 (where θ_L il the occupancy of large – size cavities, while θ_S is the same for the small – size 5^{12} cages), proving that methane is capable to fit both the types of cavities approximately in the same way [29]. Differently, the cage occupancy ratio for carbon dioxide molecules is equal to 3.12 [29]. It means that CO_2 mainly occupies the large cavities, while it is difficult to obtain high occupancy degree of large cavities for this species [30]. Consequently, the replacement process, mainly interests the large $5^{12}6^2$ cavities. It was already established that the recovery of methane, via replacement techniques carried out with pure carbon dioxide, cannot exceed 75% [2].

Moreover, further variables can affect the process negatively, such as the diffusion of carbon dioxide in hydrate lattice and the re-formation of methane hydrates.

As a consequence of it, after replacement, the reservoir will host pure methane, pure carbon dioxide (mainly associated to the formation of ex – novo structures) and mixed CO_2/CH_4 hydrates.

Because the preservation of soils is a critical issue during field applications, this new established configuration of the deposit must be considered and analyzed in depth. Methane hydrates were found to play a key role in the cementation of sediments [31]. Espinoza and Santamarina proved that, conversely to the direct recovery of methane, the replacement process allows to drastically reduce the risk of failures and loss of stiffness [32].

While the mechanical, physical, and chemical properties of pure CH_4 and CO_2 hydrates have been widely explored and are documented in detail in the literature [33–35], few experimental data exist about mixed CO_2/CH_4 hydrates, mainly because the concentration of the two respective species, within the structure of hydrates, may vary significantly as a function of the procedure followed for the replacement and due to the process conditions.

GHs are composed mainly of water molecules forming polyhedron cage with specific structure through hydrogen bonds containing gas as guest enveloped in cage; in this structure water molecule and gas molecule interact with each other by van der Waals force [1]. For all these characteristics, to characterize GHs, Raman spectroscopy represents an important technique that is widely used for the analysis of the structure of hydrates and that permit to collect information on the mechanisms of formation and decomposition of hydrates by studying the Raman spectra. Raman analysis in fact provide data on the molecular structure based on the Raman effect where the signals are generated by the vibration and rotation of the molecules. In the Raman spectrum of the hydrate, the interaction between the host molecules and the lattice of the water molecules influences the number, intensity and position of the bands generated by each molecule and therefore, the investigations on the host lattice of water molecules can provide information on the specific interaction. The Raman spectrum is appropriate for the analysis of water, aqueous solutions, and its liquid–solid transition and for the study of the main parameters affecting the water hydrogen bonds; the translational / vibrational bands are located below 400 cm^{-1}, those related to the OH – bending bands are present at about 1600 cm^{-1}, while the most intense, closely related water molecule structure, are present in the range 3000–4000 cm^{-1}. These bands are referred to symmetric and asymmetric OH–stretching vibrations (OHs) and reflect the modifications induced by the change of phase, temperature, chemical environment and about the presence of host molecule in the hydrate's structures that can be identified by specific fingerprint [36–39].

This experimental work is focused on the replacement of methane with carbon dioxide molecules into hydrates. The process was described both macroscopically and at a molecular level. Three different typologies of hydrate were produced, analyzed, and compared among each other: (i) carbon dioxide hydrate in pure water, (ii) carbon dioxide hydrate in water and into a porous medium and (iii) CO_2/CH_4 hydrates in pure water. To define the composition of this latter typology of hydrate, two replacement tests were carried out in a small – scale apparatus, appositely designed to reproduce, on a lab – scale, a natural hydrate sediment. The first of these two tests were carried out via depressurization, while the second with thermal stimulation. The results obtained with the experiments were added to previous findings, available elsewhere in literature, and were used to establish the mixture used to produce samples for the molecular analyses of the process.

At molecular level, the investigations consisted in the microscopic analysis of surface morphology of different samples of

GHs obtained by scanning electron microscope (SEM) technique; the Raman analysis characterization permitted to confirm the gas uptake in the hydrate structures by identification of the fingerprint of CH_4 and CO_2 occupancy in the hydrates, revealing the main characteristics of water forming the GHs structure in the different conditions and the interaction between the host molecule and the lattice of water molecules.

2. Methods

2.1. Experimental apparatus

The apparatus mainly consists of a 316SS lab – scale unstirred reactor, a cooling room, a series of sensors used to monitor the thermodynamic variables of the process and supplementary devices, required for the injection and ejection of gas. The reactor has cylindrical shape, and the internal volume is equal to 1000 cm^3. The shape was chosen to ensure the thermal uniformity of the internal volume, being the heat provided and/or removed from the external. In particular, the internal diameter is equal to 7.79 cm, while its height is 21 cm. Fig. 1 shows in detail the geometry of the reactor. The reactor is also equipped with an integrated coil, which allows to quickly increase or decrease the temperature, when required.

The lower section is closed with a 3 cm thickness plate, directly sealed to the perimetral wall. The top is closed with a flange, whose tightness is ensured with a spiro – metallic gasket (model DN80 PN 10/40 316-FG C8 OR).

The injection of gas is made from the bottom, where two channels are directly connected to cylinders containing the two respective species. The cylinders are positioned inside the cooling room and the guest compound has the same temperature of the system when it is injected inside the reactor. The injection from the bottom ensures a higher diffusion of the guest in the pores of sand. The flange has five channels and hosts all the sensors, a safety valve (model E10 LS/150) and the gas ejection valve. This latter element is equipped with a sub – channel, separated from the main one with a pressure reduced. It allows to isolate little quantities of gas which, thanks to the presence of a porous septum, can be withdrawn and used for gas chromatographic analyses.

The temperature was measured with six Type K thermocouples, having class accuracy 1 (uncertainty equal to ±0.01 °C), while the pressure was monitored with a manometer, model MAN – SD, having a class accuracy equal to ±0.5 of full scale. The positioning of thermocouples allows to identify with accuracy the formation of temperature gradients; it was designed according to what reported in literature for similar apparatuses [41–43]. The cooling room can lower the temperature until reaching – 10 °C, with an accuracy equal to ±0.1 °C. The scheme of the completely assembled experimental apparatus is provided in Fig. 2.

Finally, all the sensors are connected to a data acquisition system provided by National Instruments and managed in LabView.

2.2. Materials

To carry out the replacement experiments, the reactor was filled with 270 cm^3 of pure demineralized water and 800 cm^3 of sand. The sand is composed by pure silica grains, having spherical shape and diameter in the range of 150 – 250 μm. The porosity of the whole sediment was measured with a porosimeter, model Thermo Scientific Pascal 140 and is equal to 34%. This value considers both the volume of sand pores and the space present between grains. Conversely, the samples used for molecular analyses, where carried out in the only presence of water, in order to characterize the different structure and composition of CO_2/CH_4 hydrates independently from the morphology and composition of the sediment used. The experiments were carried out with Ultra-High-Purity (UHP) gases, having a certified purity degree equal to 99.99%.

2.3. Methods

The apparatus described in Section 2.1, was used to produce the three different typologies of hydrates, then used for the Raman analyses. The following structures were selected and produced: CO_2 hydrate in pure water (CO_2GHs), CO_2 hydrate in water and sand ($CO_{2(sand)}$GHs) and CO_2/CH_4 hydrate in pure water ((CH_4/CO_2)GHs).

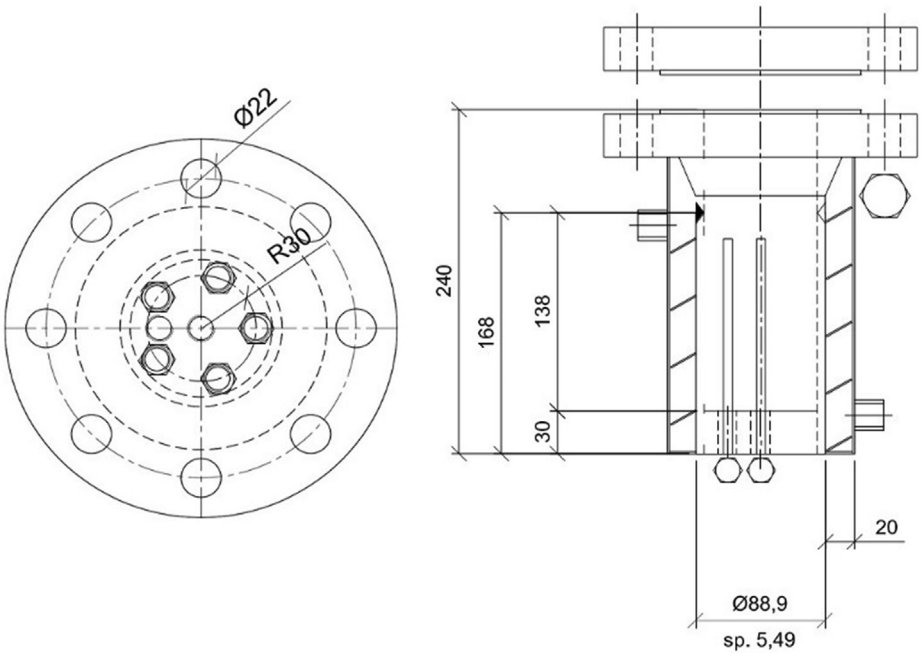

Fig. 1. Technical scheme of the reactor [40].

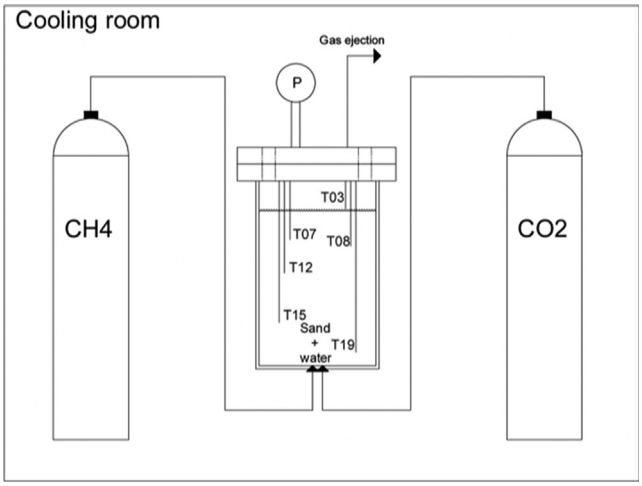

Fig. 2. Scheme of the completely assembled experimental apparatus [36].

The first two samples involved a single gaseous species, and their formation was obtained according to previous research [16,41]. The production of the third sample of hydrate prior required the definition of the composition of the gaseous phase contained into water cages. However, the accurate evaluation of such composition requires the partial dissociation of hydrates (to get material for gas analyses) and inevitably reduces the accuracy and composition of the following Raman analyses. This problem was solved by carrying out two CO_2/CH_4 replacement tests, one via depressurization and one via thermal stimulation. The hydrates phase, obtained at the end of these experiments, was then isolated, and dissociated. The gaseous phase was analyzed and, the following gas – chromatographic analysis allowed us to define the gas – composition of the third sample of hydrate used for the Raman analyses.

2.3.1. Depressurization

Starting from the equilibrium conditions, spontaneously established in the system at the end of the formation phase, the pressure was decreased about some bars, in order to produce a configuration of instability for methane hydrates. At the same time, the injection and ejection valves were opened and the gaseous phase, existing upon methane hydrates was replaced with a new CO_2/CH_4 mixture. To do this, a flow of pure carbon dioxide was inserted in the reactor, while a mixture containing both the species was ejected. Thanks to this solution, it was possible to produce a gaseous phase having a concentration in CO_2 up to 80 vol%. It was preferred to carry out the replacement process with a mixture of both species instead of pure carbon dioxide, to better represent what effectively happens in field applications. The reactor was then closed, and a sample of gas was withdrawn to measure the composition of the gaseous phase immediately after the beginning of the replacement process. The analyses of gases were made with a gas – chromatograph, model VARIAN CP 4900 Micro-GC. The concentration of methane was detected with the column Molsieve 5A, while carbon dioxide with the column Poraplot PPU. The most relevant properties of these column are shown in Table 1.

The evolution of CO_2/CH_4 exchange cannot be monitored with pressure, because of the contemporary occurrence of two opposite phenomena: the release of methane and the capture of carbon dioxide. For this reason, the process was kept free to evolve for a limited time period, whose duration was defined according to what observed in previous studies carried out with the same apparatus.

Finally, the reactor was opened, and the gaseous phase was completely removed. Then it was closed again, and the solid phase

Table 1
Main specification about the two columns used to measure the concentration of CO_2 and CH_4.

Species	Carbon dioxide	Methane
Column	Poraplot PPU	Molsieve 5A
ID	0.53 [mm]	
Length	10 [m]	
Film	20 [μm]	
Configuration	7 in. cage	
Carier gas	He	
Input pressure	550 ± 10 KPa (80 ± 1.5 psig)	
Inlet connection	3.2 mm (1/8 in.) SS compression fitting	

dissociated completely and release the gases contained in it. A second gas chromatographic analysis allowed to define the composition of hydrates formed during the experiment.

2.3.1.1. Thermal stimulation. This second solution is based on increasing the local temperature while keeping the pressure substantially unchanged. By using the integrated coil, the internal temperature was quickly increased, and, at the same time, carbon dioxide was injected in the system (the same procedure, described in the previous section, was followed). Two gas analyses were made: the first to measure the composition in the gaseous phase before the replacement and the second to evaluate the composition of hydrates at the end of the process. Except for the solution adopted to vary the local thermodynamic conditions, the same procedure of the previous section was followed.

2.4. Morphological study by SEM

The collected specimens of GHs were examined by means of a scanning electron microscope (Field Emission SEM, Sigma 300, Zeiss) coupled with an energy dispersive X-ray spectrometer (EDX, Quantax, EDS, Bruker) and with a temperature-controlled equipment (Coolstage by Seben) that allows to acquire SEM images up to the temperature of −30 °C [42].

2.5. Raman setup

A Horiba iHR-320 Raman spectrometer coupled with an Olympus microscope through two optical fibers was used in this study (the setup is schematized in Fig. 1a). This system uses the 532 nm line (max power 50mW) of a DPSS laser for excitation and has Stokes-Raman shifted spectral coverage of 70–6700 cm-1. We used a 50x microscopic objective (NA = 0.50) in order to focus the laser beam (5 μm in diameter) onto the sample and to collect the Raman photons produced by the sample in backscattering configuration. Our Raman setup included also a Linkam THMS600 commercial microscope stage for heat/freeze our samples (temp range 195 °C 600 °C). The genuine Linkam quartz sample holder was too thin for our samples and therefore we designed and developed a new sample holder in copper (Fig. 3b) having a bigger volume. The spectra we collected by using this modified system, have been recorded at two different temperatures (-15 °C and 15 °C) and the total acquisition time for each spectrum was 300 s.

3. Results and discussions

This experimental section is divided in two main subsections: the first describe the CH_4/CO_2 replacement process, carried out in the lab – scale apparatus shown in the previous paragraphs. The results, in terms of concentration of the two gaseous species in the hydrate phase, obtained in the replacement tests, was used

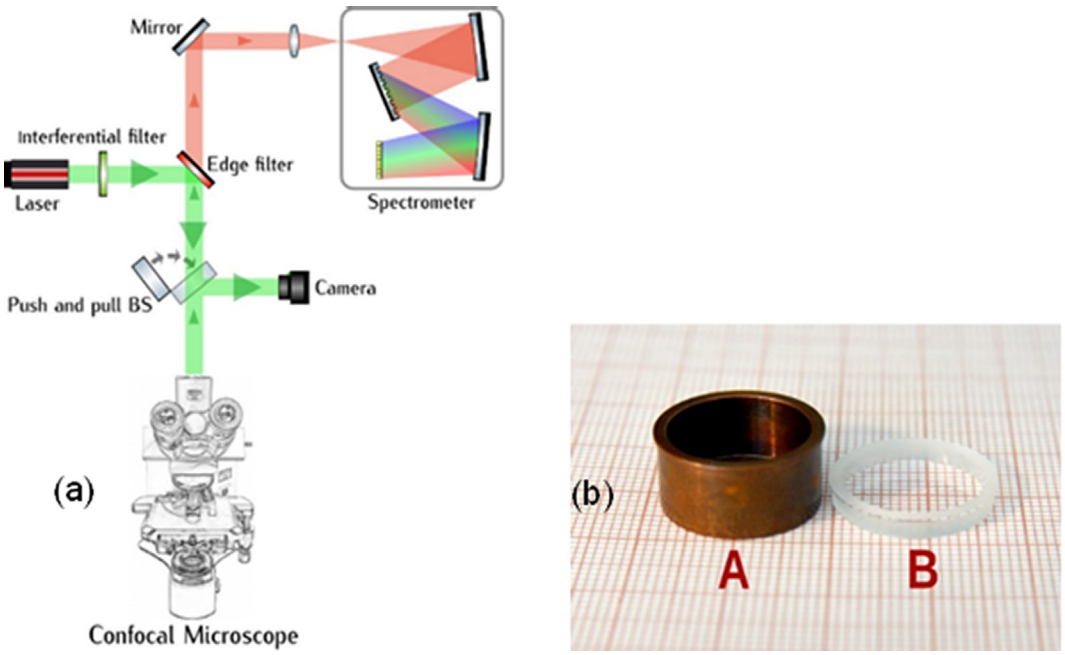

Fig. 3. (a) Raman setup; (b) Linkam sample holders (A: in copper; B in quartz).

to produce the samples analyzed in this section. The second section shows a detailed report about the SEM and Raman characterization of the GHs samples.

3.1. CO_2/CH_4 replacement tests

In this section, two replacement tests are shown. The first was carried out via depressurization, while the second with thermal stimulation.

The pressure and temperature trend over time was measured and reported for both experiments: Fig. 4a,b describe the test made with depressurization, which will be defined as Test DP, while Fig. 4b,c are related to the test made with thermal stimulation, or Test TS. Finally, Table 2 contains all the parameters of interest, directly measured, or calculated during the tests.

In addition to the data showed in Table 2, the time duration of the replacement phase was approximately equal to 30 h in both the experiments. In the diagrams, it was shortened because, start-

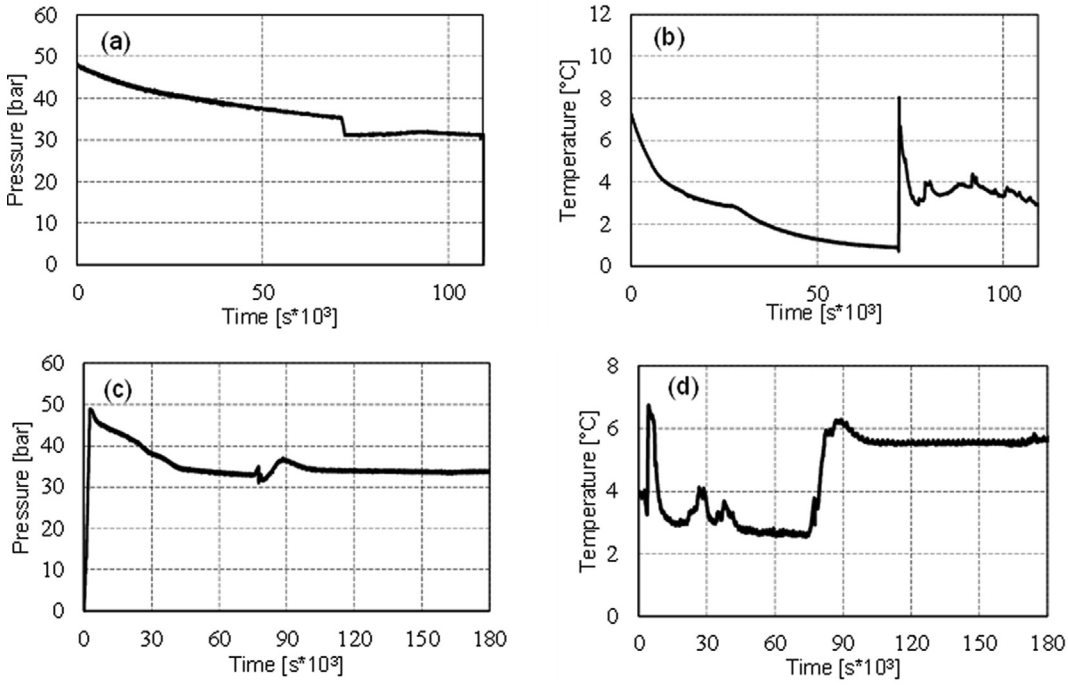

Fig. 4. (a) Pressure evolution over time in Test DP; (b) Temperature evolution over time in Test DP; (c)Pressure evolution over time in Test TS; (d) Temperature evolution over time in Test TS.

Table 2
Main parameters describing the two replacement tests.

Test	P_i [bar]	T_i [°C]	P_f [bar]	T_f [°C]	P_{repi} [bar]	T_{repi} [°C]	$\%CO_{2i}$ [Vol%]	$\%CH_{4i}$ [Vol%]	P_{repf} [bar]	T_{repi} [°C]	$\%CO_{2f}$ [Vol%]	$\%CH_{4f}$ [Vol%]
DP	47.89	7.1	35.07	0.9	31.16	2.9	82.69	17.32	31.14	3.3	71.41	28.59
TS	48.74	6.7	32.79	2.6	32.34	6.3	84.31	15.69	33.44	5.7	70.89	29.11

ing from the last values showed, the thermodynamic conditions remained unvaried until the ending of the process.

The initial formation of methane hydrates, substantially occurred in the same way in all the tests, while a different procedure was applied for the replacement phase. The one adopted in Test DP is well visible in Fig. 4a, where the evolution of pressure over time in shown in detail. Conversely, the strategy used in Test TS clearly appears in Fig. 4d.

In Test DP, immediately after the initial drop, the pressure slightly increased again and then remained stable along the whole replacement process. Nevertheless, the following gas chromatographic analysis revealed the high efficiency of the replacement, being the concentration of carbon dioxide in the hydrates phase, higher than 70 vol%. This confirms that the evolution of pressure cannot be exploited to define the evolution and the efficiency of the replacement process. The initial increase of pressure proved that, immediately after the CO_2 injection phase, the release of methane from hydrates was higher than the capture of carbon dioxide. However, the capture of CO_2 occurred from the beginning, as proved by the relevant peak in temperature, measured as soon as the injection phase finished. After that peak, the temperature returned to its previous values (it was kept slightly above the value assumed during the methane hydrates formation phase, in order to favor the replacement process). Test TS was performed with the opposite procedure. The pressure remained unchanged before and after the CO_2 injection phase. Also, this test shows an initial increase of pressure and a following stabilization. The increase in temperature is mainly associated to the thermal energy provided from the external: differently from the one observed in Test DP, the peak required some minutes to occur, then the temperature remained constant for the whole process.

The conversion of hydrates was high in both the experiments: at the end of replacement, the hydrate phase contained 71.41 vol % CO_2 in Test DP and 70.89 vol% CO_2 in Test TS. The similarity of the achieved results can be attributed to several factors: (i) the formation of methane hydrates was carried out in the same way; (ii) the concentration of carbon dioxide in the gaseous phase before replacement is similar (82.69 vol% in Test DP and 84.31 vol% in Test TS); (iii) the time was not a limiting factor.

The final concentration of carbon dioxide in the hydrate phase is high, especially if considering that the maximum concentration, which can be achieved with pure carbon dioxide, is approximately equal to 75% [1,2]. However, as previously explained, the excess of water and free space in the reactor, might have led to the formation of carbon dioxide hydrates independently from the replacement process. Therefore, the percentage obtained with the gas chromatographic analyses might overestimate the efficiency of the process. This last consideration, together with the necessity of characterizing in detail the composition and morphology of the sediment once the process is finished, justify the analyses carried out in the following section.

3.2. Gas hydrates characterization

3.2.1. Morphological study by SEM.

The study of the surface morphology and the shape of pores of gas hydrates is of great importance in understanding its morphological and physical properties and the influence of experimental conditions on their formation. To this pourpose, temperature-controlled SEM observation expresses clear differences in the micro-shapes between the various GHs samples, showing that the surface morphology changed with the specific hydrate composition. For instance, in the Fig. 5, the SEM images of different GHs at different magnifications are reported.

Specifically, at low magnification, the surface of CO_2GHs (Fig. 5a) is in the form of spherules having dimensions of the order of tens of micrometres formed from CO_2 diffusion during hydrate formation; higher magnifications of the same sample (Fig. 5b) highlight the particular shapes of the cavities in which holes are present, probably deriving from the escape of the gas promoted by the interaction with the electron beam of the microscope. For this type of GH, the only presence of CO_2 and water promoted the formation of grains uniform in size.

When the GHs are formed in presence of sediments, as in the $CO_{2(sand)}$GHs (Fig. 5c,d), a profound change in the morphology can be observed in comparison with that of the GHs formed without sediments, showing densely packed crystals separated from empty spaces; this morphology is more compact and presents similarity to that of natural gas hydrates where the sediments are present [44].

Finally, (CH_4/CO_2)GHs (Fig. 5e,f) shows a more organised texture with a mixture of different morphologies in which particular shapes can be evidenced, that are similar to those present on CO_2-GHs; the characteristics of these GHs highligt an increase in the specific surface area of the hydrate, which probably can permit to enhance the adsorption surface of gas molecules promoting the hydrate formation.

All these results demonstrated as the hydrate surface morphology clearly changed in the different experimental conditions. In particular, different organizations of water molecules forming the hydrate crystals depended on the gas composition and of the presence of sediments; all the different parameters influence in fact the nucleation mode of water crystals forming the respective GHs.

3.2.2. Raman analysis

Fig. 6 shows a typical Raman spectrum collected from CO_2GHs at 213 K. The graph demonstrates the presence of two peaks in the region 1200–1400 cm^{-1}, which correspond to the well-known Fermi-diad peaks of CO_2 in hydrate structure [45]; the respective peak positions, of stretching vibration C−O (ν1) and the overtone of the folding modes O-C-O (2ν2), are present at 1271,1 and 1375,3 cm^{-1} respectively. The range of frequencies between 2800 and 3800 cm^{-1} are closely related to the structure of water and are referred to O−H stretching bands. This broad band of water is a sum of several overlapping bands, which are, the symmetrical and asymmetrical stretching vibrations of hydrogen bonded water molecules present at about 3150 cm^{-1} and 3410 cm^{-1} respectively, and also the symmetric and asymmetric stretching vibration of unbounded water molecules observed at about 3540 cm^{-1} and 3620 cm^{-1} respectively [45].

Furthermore, when the measurements were performed at increasing temperatures, no change and no shift of CO_2 bands were observed from the analysis of this sample but, however, CO_2 bands disappeared at temperatures above 263 K due to the complete release of the gas.

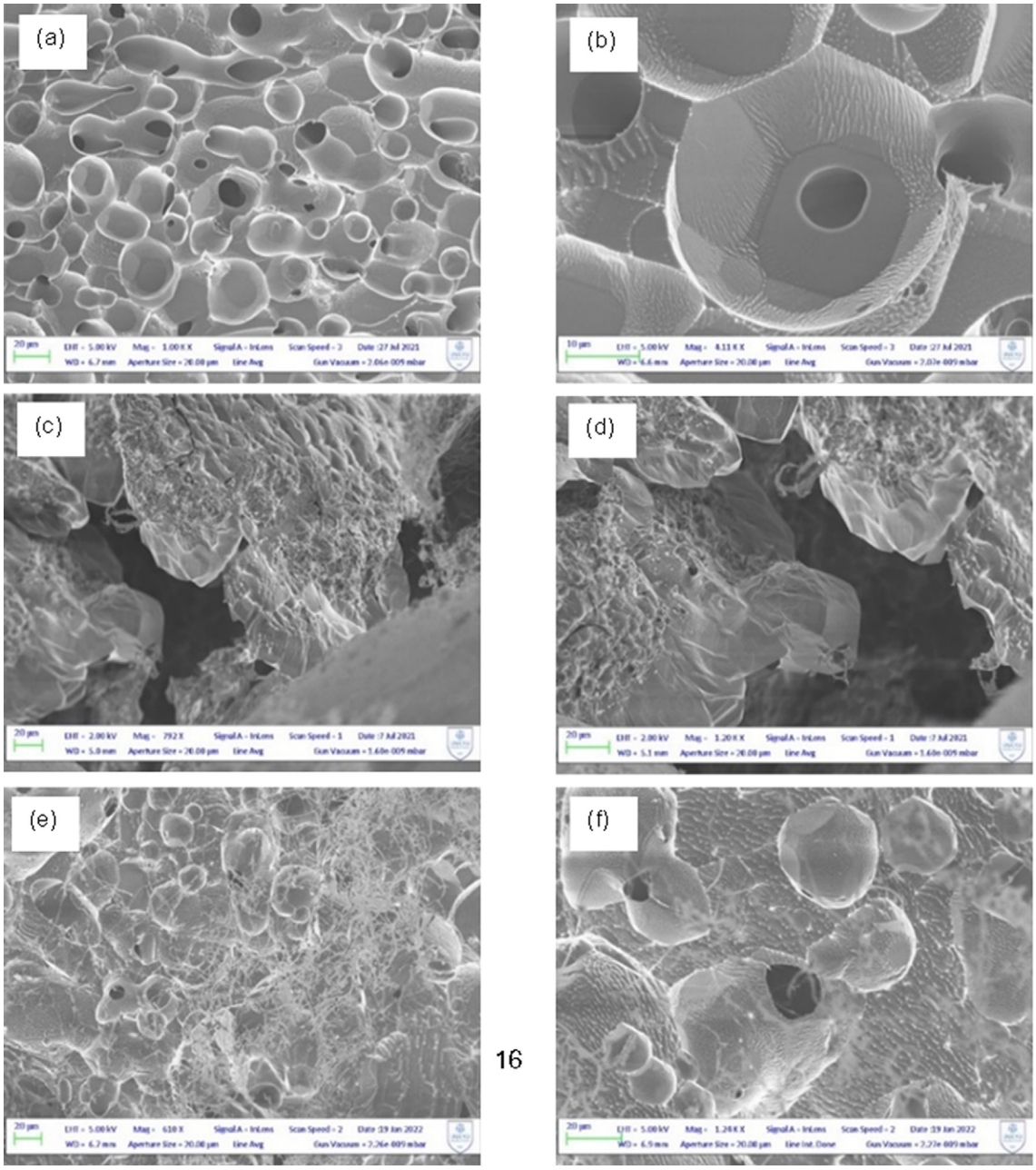

Fig. 5. SEM images showing the surface morphology of CO_2GH (a,b), $CO_{2(sand)}$GHs (c,d), (CH_4/CO_2)GHs (e,f).

Important information can be obtained from the observation of O–H stretching bands (OHs) of water that are related to the formation of relative hydrogen bonds; the modifications in the global profile of Raman spectra can in fact reflect the changes in the physical and chemical properties of water molecules in the hydrate structure. Interesting details can be collected by the calculation of the area under the Raman spectrum in the range 3000–3600 cm^{-1} after the division in two sections around the center of the O—Hs bands that is located at 3325 cm^{-1} and that represents the isosbestic point; the lower frequency part of the spectrum corresponds to symmetric OHs bands while the higher is related to asymmetric OHs bands and it is possible to control the relative evolution of the two sections of the O—Hs regions as the change of the order/disorder of the water structure [47].

As can be observed from the Fig. 7a (for CO_2GHs) and Fig. 7b (for $CO_{2(sand)}$GHs), the increasing in temperature induced evident changes in the shape and in the intensity of the O—Hs bands; in fact, the left bands (called A) decreases and red shifted while the right bands (called B) slightly red shifted. The ratio between the corresponding integrated intensities of the two regions (B/A) represent S_D index [45]. It easy to observe as the obtained results show a direct correlations of S_D index with the increase of temperature (Fig. 7c); in this case, the symmetrical contribution of the OHs bands is higher in pure water (lower S_D) as compared to that in the presence of sand (higher S_D), demonstrating in the latter, a marked interference in the organization of the water molecules to form in this case, less ordered structures. However, it should be noted that the $CO_{2(sand)}$GHs (violet straight line on Fig. 7c), is less influenced from the increase of temperature when compared to that obtained from hydrate of pure water (green straight line on Fig. 7c). This could mean that the sand attenuates the modification of hydrate structure, due probably to the interaction between

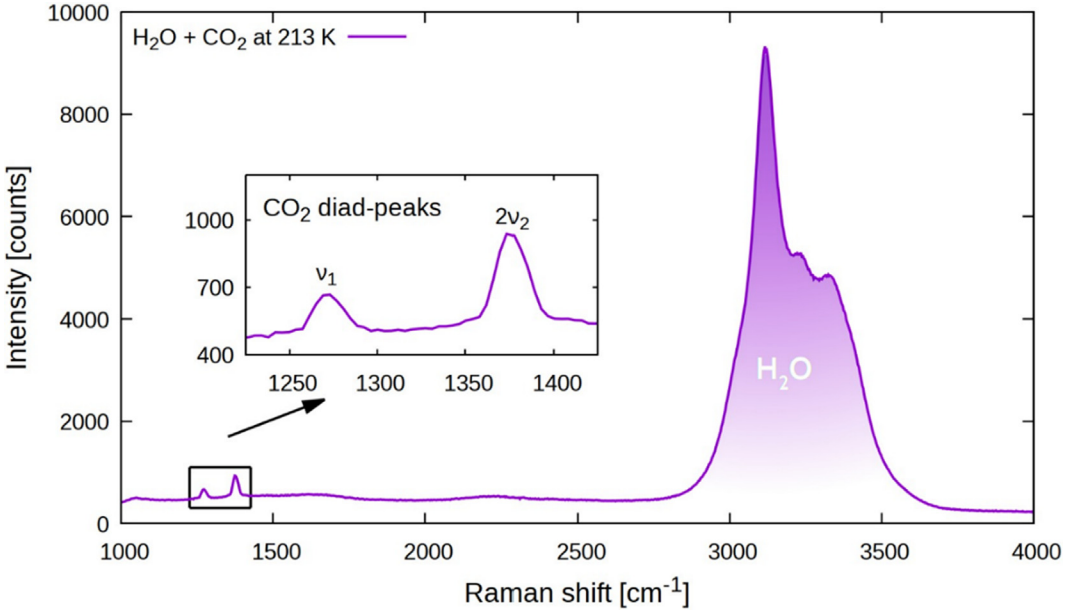

Fig. 6. Raman spectra of CO_2GH at 213 K showing the CO_2 Fermi- peaks (see zoom in the insert of figure) and symmetric and asymmetric OHs bands of water.

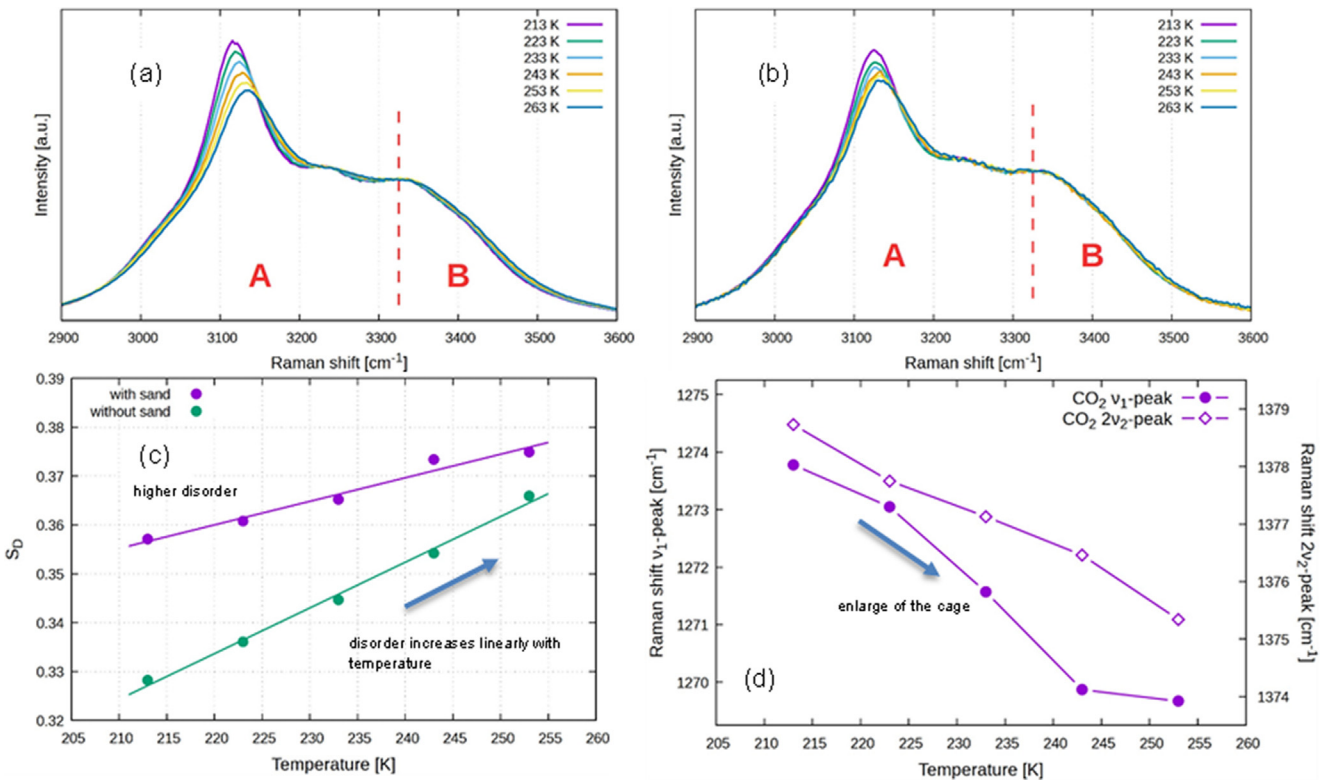

Fig. 7. Raman spectra of OHs vibration bands at different temperatures of CO_2GHs (a) and $CO_{2(sand)}$GHs (b); correlation of S_D concentration index as function of change in temperatures (c) Raman shift of CO_2 Fermi diad at different temperatures of CO_2GHs_sand (d).

silanol groups of sand particles and water molecules. It is in fact previously proved that the water molecules, located on the silicate surface of sediments, induce intermolecular hydrogen bonding interaction with silanol groups [45,48].

Moreover, as reported in Fig. 7d, the CO_2 Fermi-diad peaks in the presence of sand, demonstrates a linear blue shift with the increase of temperature. In general, since the larger is the cage diameter, the smaller is the Raman shift [49], this result can be probably due to an enlarge of the cage respect to the same in the absence of sand due to the temperature increase. In this case, it is reasonable to think that the less rigid structure of this hydrate, due to the presence of sand, together with its maintenance in the studied temperature range, favored therefore the formation of expansion process; on the contrary, with pure water, the expan-

sion of the cells was contained due to more compact texture of this GH. These results reflected the changes in the physical chemical properties of water molecules in the hydrate phase in the presence of sand that can be also correlated to the behavior of CO_2 as guest molecule.

The Raman spectrum of CH_4/CO_2 mixed hydrates formed by replacement, reported in Fig. 8, shows both the characteristic signal of the methane and of the carbon dioxide inside the hydrates. Specifically, CH_4 signals, that represent the symmetric C – H stretching of CH_4 in large cages and in small cages, are located at 2905,4 and 2916,4 cm^{-1} respectively, and CO_2 Fermi-diad peaks are presents at 1277,5 and 1382,0 respectively; moreover, in the spectrum, the small signal at around 2300 cm^{-1} can be attributed to the N_2 signal that is present because GHs samples are collected into liquid N_2 that is used to maintain the sample at low temperature during transport to the laboratory.

The relative shift positions of CO_2 and CH_4 signals observed in the Raman spectra of all GHs (Table 3) were around the range of values present in the literature data proving the efficiency of the preparation conditions of all GHs [46,50]; however, the differences in the shift positions can be interpretated and attributed to the different composition of GHs. In fact, the Raman shifts of CO_2 characteristic signals for CO_2GHs in pure water at 1271.1 and 1375.3 cm^{-1}, red shifted in the presence of sand and more, in the co-presence of CH_4; specifically, the obtained values of the Raman shifts can indicate small difference in the size of the cages in the studied GHs, with the smaller cages on (CH_4/CO_2)GHs and higher cages on CO_2GHs [49].

On the other and, the data obtained by Raman spectra cannot be directly correlated with the quantity of CO_2 inside the GHs structure that instead can be estimated from the ratio of the peak total areas (integral intensity) of the two CO_2 signals and that of water (CO_2/H_2O); in fact, the integral area of the bands reflects the number of guest molecules within the Raman cross-section [51].

In order to compare the different results, in Fig. 9a the spectra of all samples, normalized on the isosbestic point of the water spectra, are reported to illustrate the abundance of CO_2 in the different GHs. In this case, the calculation of the CO_2/H_2O area ratio for the different GHs permits to define the CO_2 abundance order in the different GHs as reported in Table 3. The results indicate that the richest in CO_2 is (CH_4/CO_2)GHs (area ratio of 0.0244) while the poorest are CO_2GHs and $CO_{2(sand)}$GHs (area ratios of 0.0071 and 0.0093 respectively).

Furthermore, as can be observed from the data reported in Table 3, in the regard of the CO_2 signals, the vibrational contribution (2ν2) is about double when compared to that of stretching (ν1) for everyone GH. Because it has been observed that the peak positions of the Fermi diad and the (2ν2)/(ν1) area ratio of CO_2 vary with density [52], another interesting consideration can be highlighted from these results that evidence as, to higher (2ν2)/(ν1) area ratio that is obtained of (CH_4/CO_2)GHs, corresponds higher CO_2 amount.

It is also interesting to compare the spectral data of the three types of GHs measured at the same temperature; in the Fig. 9b is easy to observe the important differences related to symmetric contribute of OHs bands that are numerically expressed from the S_D values and that represent a description of the order/disorder property of water in the GHs structure. In this case, the obtained S_D values show that the least ordered water structure in the hydrate is that in which sand is present, while the most ordered one is that in the presence of CO_2 and methane. This last result, together to the abundance of CO_2 inside the (CH_4/CO_2)GHs, allows to conclude that the contemporary presence of both species (CO_2 and CH_4) provides to the hydrate lattice even more strength than that of hydrates containing a single species. The theoretical explanation can be found at the microscopic level: both typologies of guest spontaneously form sI hydrates, a structure composed by pentagonal dodecahedrons (5^{12}) and tetrakaidecahedrons ($5^{12}6^2$). While both species preferentially occupy the largest typology of

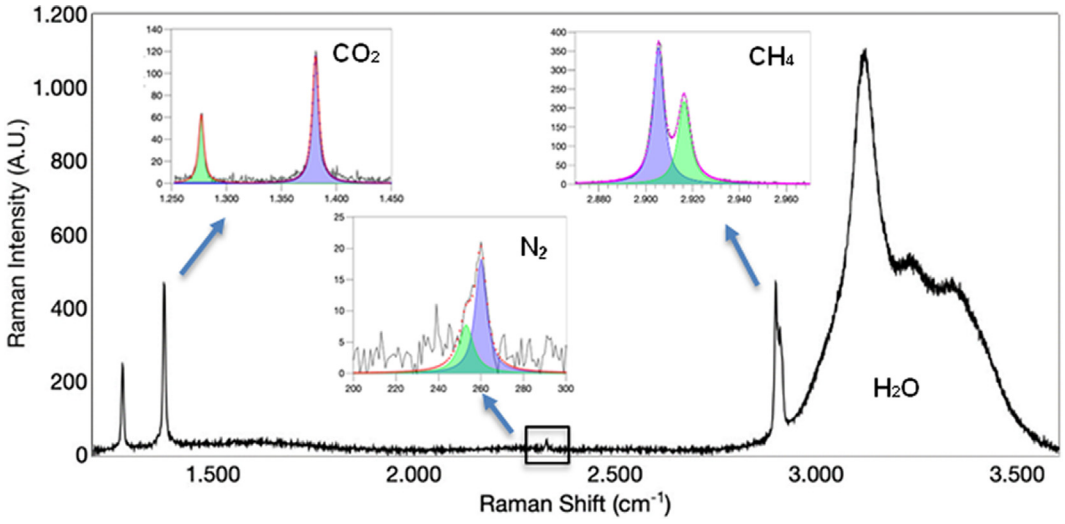

Fig. 8. Raman spectrum of (CH_4/CO_2)GHs.

Table 3
Raman shifts of CO_2 and CH_4 on GHs samples, CO_2/H_2O, and CO_2 signals area ratio at 213 K.

	CO_2 C–O (ν1) (cm^{-1})	**CO_2**O-C-O (2ν2) (cm^{-1})	**CH_4** large cage (cm^{-1})	**CH_4** small cage (cm^{-1})	**CO_2/H_2O** area ratio	**CO_2 (2ν2)/(ν1)** area ratio
CO_2GHs	1271.1	1375.3	–	–	0.0071	2.099
$CO_{2(sand)}$GHs	1272.3	1377.5	–	–	0.0093	2.075
(CH_4/CO_2)GHs	1277.5	1382.0	2905.4	2916.4	0.0244	2.217

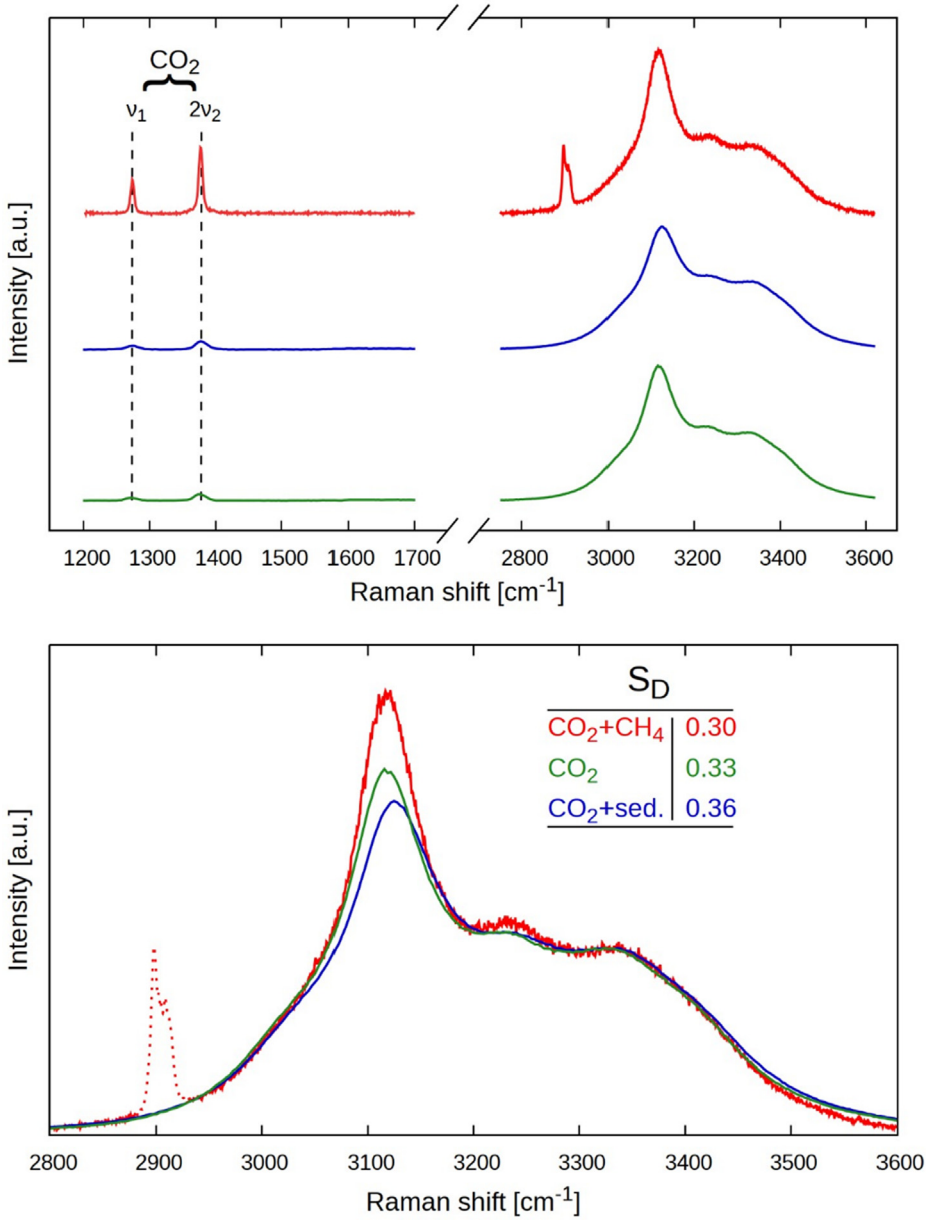

Fig. 9. Normalized Raman spectra of CO_2GHs (green line), $CO_{2(sand)}$GHs (blue line) and (CH_4/CO_2)GHs (red line) with evidenced S_D values (213 K). In the S_D calculation the area related to methane (signed as dotted line) is not considered.

cavity (or the second cited) it is more difficult for carbon dioxide molecules (compared with methane molecules) to occupy the small 5^{12} cavities. It leads to a higher hydration number and to a general lower stability of the hydrate lattice. Conversely, both types of molecules easily enter in the $5^{12}6^2$ cavities, but the greater size of CO_2 allows to completely fill the cavity and ensures higher stability and strength [1]. In fact, the ratio between molecular diameter and cavity diameter is, for the tetrakaidekahedral structure, equal to 0.744 for methane and to 0.834 for carbon dioxide [1]. Being this latter value closer to one, the presence of carbon dioxide within this type of cavity produces higher stability and strength. It means that, the presence of both types of molecules within the hydrate lattice allows to improve the fitting of each cavity, reduce the percentage of empty cages and, consequently, the hydration number, with quantifiable advantages in terms of stability and strength of the whole structure.

4. Conclusions

The process of the replacement of methane with carbon dioxide molecules into hydrates was described both macroscopically and at a molecular level by studying three different typologies of hydrate. SEM observation showed that the surface morphology of GHs changed with the specific hydrate composition and that larger surface morphology is present on (CH_4/CO_2)GHs.

The Raman measurements, through the study of fingerprint of host molecules and of water OHs bands, permitted to evaluate properties and behavior of the different GHs. Specifically, the CO_2 hydrates showed a less ordered structure in the presence of sand but however, thanks to the interaction between water and silanol groups of sand particles, their stability was maintained with the variation of temperature, favoring the expansion of the cages that was highlighted by the shifts of the CO_2 Fermi diad. The calculated

S_D indices correlated perfectly with the increase of temperature but also provided information about the characteristics of water inside GHs, showing that the least ordered water structure was present on $CO_{2(sand)}$GHs, while the most ordered one was that of (CH_4/CO_2)GHs.

In addition, by these measurements, (CH_4/CO_2)GHs was proved to contain the most quantity of CO_2 confirming therefore a favorable replacement of methane and that the process provided to the hydrate lattice even more strength than that of hydrates containing a single species; these results were in accordance with larger surface morphology observed with SEM measurements.

The collected information provided a better understanding of as, a careful observation of the Raman spectra of GHs, can improve the knowledge on complex phase behavior, on specific occupation of the cages of external host molecules and on the characteristics of the mixed gas hydrates.

These results add other elements to the information in the literature for the dual purpose of CH_4 recovery and CO_2 sequestration, also underlining the fact that the kinetics and the extent of replacement in actual natural gas hydrate reservoirs are strictly dependent on various factors such as characteristics of sediment, temperature, hydrate structure and generally on environmental characteristics in which hydrates are present.

CRediT authorship contribution statement

Rita Giovannetti: Funding acquisition, Project administration, Conceptualization, Supervision, Writing – review & editing. **Alberto Maria Gambelli:** Methodology, Formal analysis, Data curation, Writing – review & editing. **Andrea Rossi:** Conceptualization, Methodology, Writing – review & editing. **Beatrice Castellani:** Methodology, Formal analysis, Data curation. **Marco Minicucci:** Methodology, Formal analysis, Data curation. **Marco Zannotti:** Methodology, Formal analysis, Data curation. **Andrea Nicolini:** Methodology, Writing – review & editing. **Federico Rossi:** Funding acquisition, Project administration, Supervision.

Data availability

No data was used for the research described in the article.

Declaration of Competing Interest

The authors declare that they have no known competing financial interests or personal relationships that could have appeared to influence the work reported in this paper.

Acknowledgements

The authors gratefully acknowledge financial support derived by the PRIN Project entitled: "Methane recovery and carbon dioxide disposal in natural gas hydrate reservoirs". The authors gratefully acknowledge the School of Science of and Technology of University of Camerino for providing important technical and scientific resources such as the field-emission SEM (Sigma 300) and the customized micro-Raman spectroscopy equipment (Olympus-Horiba iHR320), necessary for this work.

References

[1] Sloan ED, Koh CA. Clathrate hydrates of natural gases. Third Ed, CRC Press, Boca Raton, FL USA, 2007.
[2] A.M. Gambelli, A. Presciutti, F. Rossi, Review on the characteristics and advantages related to the use of flue – gas as CO_2/N_2 mixture for gas hydrate production, Fluid Phase Equilib. 541 (2021).
[3] T. Collett, Energy resource potential of natural gas hydrates, AAPG Bull. 86 (2002) 1971–1992.
[4] X.Y. Li, X.S. Li, Y. Wang, J.W. Liu, H.Q. Hu, The optimization mechanism for gas hydrate dissociation by depressurization in the sediment with different water saturations and different particle sizes, Energy 215 (2021).
[5] X.S. Li, C.G. Xu, Y. Zhang, X.K. Ruan, G. Li, Y. Wang, Investigation into gas production from natural gas hydrate: a review, Appl. Energy 172 (2016) 286–322.
[6] P.A.J. Donkers, L.C. Sogutoglu, H.P. Huinink, H.R. Fischer, O.C.G. Adan, A review of salt hydrates for seasonal heat storage in domestic applications, Appl. Energy 199 (2017) 45–68.
[7] X. Wang, F. Zhang, W. Lipinski, Research progress and challenges in hydrate – based carbon dioxide capture applications, Appl. Energy 269 (2020).
[8] C.A. Koh, E.D. Sloan, Natural gas hydrates: recent advances and challenges in energy and environmental applications, AIChE J. 53 (2007) 1636–1643.
[9] V.C. Nair, S.K. Prasad, R. Kumar, J.S. Sangway, Energy recovery from simulated clayey gas hydrate reservoir using depressurization by constant rate gas release, thermal stimulation and their combination, Appl. Energy 225 (2018) 755–768.
[10] J. He, X. Li, Z. Chen, Q. Li, Y. Zhang, Y. Wang, Z. Xia, C. You, Combined styles of depressurization and electrical heating for methane hydrate production, Appl. Energy 282 (2021).
[11] A.M. Gambelli, Analyses on CH_4 and CO_2 hydrate formation to define the optimal pressure for CO_2 injection to maximize the replacement efficiency into natural gas hydrate in presence of a silica – based natural porous medium, via depressurization, Chem. Eng. Process. – Process Intens. 167 (2021).
[12] K. Xuan, W. Yi, X.S. Li, Y. Zhang, Z.Y. Chen, Influence of heat conduction and heat convection on hydrate dissociation by depressurization in a pilot – scale hydrate simulator, Appl. Energy 251 (2019).
[13] Y. Wang, J.C. Feng, X.S. Li, Y. Zhang, Experimental investigation of optimization of well spacing for gas recovery from methane hydrate reservoir in sandy sediment by heat stimulation, Appl. Energy 207 (2017) 562–572.
[14] J.C. Feng, Y. Wang, X.S. Li, Hydrate dissociation induced by depressurization in conjunction with warm brine stimulation in cubic hydrate simulator with silica sand, Appl. Energy 174 (2016) 81–91.
[15] S.S. Tupsakhare, M.J. Castaldi, Efficiency enhancements in methane recovery from natural gas hydrates using injection of CO_2/N_2 gas mixture simulating in – situ combustion, Appl. Energy 236 (2019) 825–836.
[16] A.M. Gambelli, F. Rossi, Natural gas hydrates: comparison between two different applications of thermal stimulation for performing CO_2 replacement, Energy 172 (2019).
[17] T.S. Collett, G.D. Ginsburg, Gas hydrates in the Messoyakha gas field of the west Siberian basin – a re – examination of the geologic evidence, International Journal of Offshore Polar Engineers 8 (1997) 96–103.
[18] T.S. Collett, V.A. Kuuskraa, Hydrates contain vast store of world gas resources, Oil Gas J. 96 (1998) 90–95.
[19] Z.Y. Chen, Q.P. Li, Z.Y. Yan, K.F. Yan, Z.Y. Zeng, X.S. Li, Phase equilibrium and dissociation enthalpies for cyclopentane plus methane hydrates in NaCl aqueous solutions, J. Chem. Eng. Data 55 (2010) 4444–4449.
[20] Y. Wang, J.C. Feng, X.S. Li, L. Zhan, X.Y. Li, Pilot – scale experimental evaluation of gas recovery from methane hydrate using cycling – depressurization scheme, Energy 160 (2018) 835–844.
[21] A. Hassanpouryouzband, E. Joonaki, M.V. Farahani, S. Takeya, C. Ruppel, J. Yang, N.J. English, J.M. Schicks, K. Edlmann, H. Mehrabian, Z.M. Aman, B. Tohidi, Gas hydrates in sustainable chemistry, Chem. Soc. Rev. 15 (2020) 5225.
[22] A.M. Gambelli, U. Tinivella, R. Giovannetti, B. Castellani, M. Giustiniani, A. Rossi, M. Zannotti, F. Rossi, Observation of the main parameters influencing the formation of gas hydrates, Energies 14 (2021) 1803.
[23] K. Ohgaki, Y. Inoue, A proposal for gas – storage on the ocean – floor using gas hydrates, Kagaku Kogaku Ronbun 17 (1991) 1053–1055.
[24] N. Goel, In situ methane hydrate dissociation with carbon dioxide sequestration: current knowledge and issues, J. Petrol. Sci. Eng. 51 (2006) 169–184.
[25] Y. Seo, S. Lee, J. Lee, Experimental verification of methane replacement in gas hydrates by carbon dioxide, Chem. Eng. Trans. 32 (2013) 163–168.
[26] C. Deusner, N. Bigalke, E. Kossel, M. Haeckel, Methane production form gas hydrate deposits through injection of supercritical CO_2, Energies 5 (2012) 2112–2140.
[27] D.Y. Koh, H. Kang, D.O. Kim, J. Park, M. Cha, H. Lee, Recovery of methane from gas hydrates intercalated within natural sediments using CO_2 and CO_2/N_2 gas mixture, ChemSusChem 5 (2012) 1443–1448.
[28] A.M. Gambelli, F. Rossi, Thermodynamic and kinetic characterization of methane hydrate nucleation, growth and dissociation processes, according to the Labile Cluster theory, Chem. Eng. J. 425 (2021).
[29] P. Englezos, Clathrate hydrates, Ind. Eng. Chem. Res. 32 (1993) 1251–1274.
[30] F. Rossi, A.M. Gambelli, Thermodynamic phase equilibrium of single – guest hydrate and formation data of hydrate in presence of chemical additives: a review, Fluid Phase Equilib. 536 (2021).
[31] J. Yang, A. Hassanpouryouzband, B. Tohidi, E. Chuvilin, B. Bukhanov, V. Istomin, A. Cheremisin, Gas hydrates in permafrost: distinctive effect of gas hydrate and ice on the geometrical properties of simulated hydrate – bearing permafrost sediments, J. Geophys. Res. 124 (2019) 2551–2563.
[32] D.N. Espinoza, J.C. Santamarina, P-wave monitoring of hydrate – bearing sand during CH_4 – CO_2 replacement, Int. J. Greenhouse Gas Control 5 (2011) 1031–1038.
[33] W.F. Waite, W.J. Winters, D.H. Mason, Methane hydrate formation in partially water – saturated Ottawa sand, Am. Mineral. 89 (2004) 1202–1207.

[34] W.J. Winters, I.A. Pecher, W.F. Waite, D.H. Mason, Physical properties and rock physics models of sediment containing natural and laboratory – formed methane gas hydrate, Am. Mineral. 89 (2004) 1221–1227.
[35] W.J. Winters, W.F. Waite, D.H. Mason, L.Y. Gilbert, I.A. Pecher, Methane gas hydrate effect on sediment acoustic and strength properties, J. Petrol. Sci. Eng. 56 (2007) 127–135.
[36] D.M. Carey, G.M. Korenowski, Measurement of the Raman spectrum of liquid water, J. Chem. Phys. 108 (1998) 2669–2675, https://doi.org/10.1063/1.475659.
[37] W.B. Monosmith, G.E. Walrafen, Temperature dependence of the Raman OH stretching overtone from liquid water, J. Chem. Phys. 81 (1984) 669–674, https://doi.org/10.1063/1.447748.
[38] T. Shimoaka, T. Hasegawa, K. Ohno, Y. Katsumoto, Correlation between the local OH stretching vibration wavenumber and the hydrogen bonding pattern of water in a condensed phase: Quantum chemical approach to analyze the broad OH band, J. Mol. Struct. 1029 (2012) 209–216.
[39] Uchida T., Sum A.K., IR and Raman spectroscopy of clathrate hydrates, in: R. John A., A. Saman (Eds.) Clathrate Hydrates: Molecular Science and Characterization, vol. 1, Wiley Online Library, 2022, pp. 569-629.
[40] F. Rossi, Y. Li, A.M. Gambelli, Thermodynamic and kinetic description of the main effects related to the memory effect during carbon dioxide hydrates formation in a confined environment, Sustainability 13 (2021) 13797.
[41] Y. Wang, J.C. Feng, X.S. Li, Y. Zhang, Experimental investigation of optimization of well spacing for gas recovery from methane hydrate reservoir in sandy sediment be heat stimulation, Appl. Energy 207 (2017) 562–572.
[42] Q. Yuan, C.Y. Sun, X. Yang, P.C. Ma, Z.W. Ma, B. Liu, Q.L. Ma, L.Y. Yang, G.J. Chen, Recovery of methane from hydrate reservoir with gaseous carbon dioxide using a three – dimensional middle – size reactor, Energy 40 (2012) 47–58.
[43] Z. Yin, L. Huang, P. Linga, Effect of wellbore design on the production behaviour of methane hydrate – bearing sediment induced by depressurization, Appl. Energy 254 (2019).
[44] J. Sun, C. Li, X. Hao, et al., Study of the surface morphology of gas hydrate, J. Ocean Univ. China 19 (2020) 331–338.
[45] R. Giovannetti, A.M. Gambelli, B. Castellani, A. Rossi, M. Minicucci, M. Zannotti, Y. Li, F. Rossi, May sediments affect the inhibiting properties of NaCl on CH_4 and CO_2 hydrates formation? An experimental report, J. Mol. Liq. 359 (2022).
[46] L. Chen, H. Lu, J.A. Ripmeester, Raman spectroscopic study of CO_2 in hydrate cages, Chem. Eng. Sci. 138 (2015) 706–7.
[47] I. Durickovic, Using Raman spectroscopy for characterization of aqueous media and quantification of species in aqueous solution, in (Ed.), Applications of Molecular Spectroscopy to Current Research in the Chemical and Biological Sciences. IntechOpen. <https://doi.org/10.5772/64550>.
[48] F. Li, Z. Li, Y. Wang, S. Wang, X. Wang, C. Sun, Z. Men, A Raman spectroscopy study on the effects of intermolecular hydrogen bonding on water molecules absorbed by borosilicate glass surface, Spectrochim. Acta Part A Mol. Biomol. Spectrosc. 196 (2018) 317–322.
[49] W. Cai, X. Huang, H. Lu, Instrumental methods for cage occupancy estimation of gas hydrate, Energies 15 (2022) 485.
[50] Zhu Y.J., Xie Y., Jin-Rong Zhong J.R., Wang X.H., Xiao P., Sun C.Y., and Guang-Jin Chen G.J., Mini Review on Application and Outlook of In Situ Raman Spectrometry in Gas Hydrate Research Energy & Fuels Article ASAP, DOI: 10.1021/acs.energyfuels.2c01745.
[51] Huang X., Cai W., Zhan L., Hailong, Study on the reaction of methane hydrate with gaseous CO2 by Raman imaging microscopy Chemical Engineering Science (2020) 115720.
[52] W.X. Xiaolin, I.M. Chou, W. Hu, C. Robert, Burruss, Qiang Sun, Yucai Song, Raman spectroscopic measurements of CO2 density: Experimental calibration with high-pressure optical cell (HPOC) and fused silica capillary capsule (FSCC) with application to fluid inclusion observations, Geochim. Cosmochim. Acta 75 (14) (2011) 4080–4093.